PNAS

Supporting Information for

Self-regulation of the nuclear pore complex enables clogging-free crowded transport

Tiantian Zheng and Anton Zilman

Anton Zilman
E-mail: zilmana@physics.utoronto.ca

This PDF file includes:

Supporting Information Text

A. Alternative simulation set-ups.

A.1. Weakly attractive NTR-NTR interactions. The simulations in the main text assume that NTRs interact with other NTRs only through an excluded volume interaction (steric repulsion), with no attractive component ($\epsilon_{\text{attr}} = 0$ between NTRs). In order to examine how possible short-range weakly attractive interaction between NTRs would affect our results, we repeated the simulations with $\epsilon_{\text{attr}} = 0.1\ k_BT$ between NTRs. Figure S2A and B show that main features of the results remain unchanged: flux through the NPC remains non-saturating and an anti-clogging regime exists at low NTR concentrations.

A.2. Imperfect absorption at the nuclear boundary. In the model in the main text, the steady state NTR flux generated by the RanGTP cycle is approximated by a steady state flux generated by the absorbing boundary at the nuclear side where particles are absorbed and re-injected on the cytoplasmic side. To test that our results are not an artifact of the choice of the boundary conditions, we explored an alternative case where a fraction (25%) of the NTRs experienced a reflecting boundary at the nuclear end of the simulation instead of an absorbing boundary (while the absorbing boundary holds for the remaining 75% of NTRs). Figure S2C and D show that this does not change the non-saturating behavior of the flux, and the anti-clogging regime at low NTR concentrations persists.

A.3. NTR model with discrete binding "patches". One concern with using a spherically uniform NTR model is that it may not capture roughness of the effective potential on length scales smaller than the size of the NTR arising from the discrete nature of the FG nup binding sites, resulting in inaccurate or biased measurements of times (1). While a full investigation using more realistic coarse-grained models of NTRs is beyond the scope of this work, we show in Figure S3 that introducing discrete binding patches on our NTRs results in potentials which are very similar to the ones obtained using uniform NTRs in terms of smoothness and the response to crowding.

In these NTR models, the size of each patch has a diameter of 1 nm (corresponding to one monomer on the FG nups, and roughly the size of an FG repeat), and the patches are distributed in an approximate spiral pattern on the surface of the NTR (which remains a sphere of diameter 5 nm) to mimic the solenoidal shape of Importins/Karyopherins. Each binding patch interacts attractively with FG nup monomers with $\epsilon_{\text{attr}} = 2.4\ k_BT$ for 6 binding patches, $\epsilon_{\text{attr}} = 2.0\ k_BT$ for 8 binding patches, and $\epsilon_{\text{attr}} = 1.8\ k_BT$ for 10 binding patches. These values were chosen to approximately match the depths of the effective potentials in the case of uniform NTRs. The remainder of the NTR excluding these binding patches has a purely repulsive interaction with FG nups, with $\epsilon_{\text{attr}} = 0$.

B. Choice of the start and end points of the translocation attempts: effects on the anti-clogging regime. Our choice of the locations of where NTRs are considered to have left the NPC (thereby terminating abortive or successful entry events) are informed by the single molecule tracking experiments of (2). As their experiments used human NPCs, which are longer than the yeast NPCs we modelled our mimic on, we opted for definitions which were similar in motivation, rather than preserving the exact distances. Their translocation attempts terminated once the NTRs reached positions where they were no longer be expected to interact with the NPC (i.e. they were further from the nuclear envelope than the distance between the tip of the cytoplasmic filaments to the centre of the NPC). In our model, as we had no cytoplasmic filaments, we chose the point at which NTRs were considered to have left the pore to be where the entire volume of the NTR was outside of the pore. Using our pore dimensions, this placed our pore exits at $z = \pm 22.5$ nm.

In order to understand whether our results were robust to this choice, we computed the translocation probabilities and transport times using Equations 3 and 4 for different choices of the assumed NPC entry and exit locations of the NTRs. As shown in Figure S6D), the decrease of transport times due to crowding is a very robust phenomenon and is insensitive to changes in these definitions. By contrast, the increase of the probabilities with crowding is more sensitive to the entry/exit locations definitions because it depends on NTR-induced re-arrangements of the FG nup cloud near the pore entrances. Figure S6C shows that the choice for the locations of the exits can be shifted by 10 nm outward while maintaining this regime. However, as 99% of the FG nups in the model are contained within the region between $z = -40$ nm and $z = 40$ nm, shifting the exit locations beyond these values leads to the disappearance of the anti-clogging regime.

We also examined the choice of the definition of the pore entry locations as the point where the entire volume of the NTR was inside the pore (at $z = -17.5$ nm). Figure S6A and B show that shifting the definition of the pore entrance towards the cytoplasmic exit does not affect the existence of the anti-clogging regime.

C. Measuring the effective potentials and the diffusion coefficients. We ran auxiliary simulations in order to measure the effective potentials and diffusion coefficients inside the pore at different NTR concentrations. To measure

the equilibrium effective potential in the pore, we ran simulations where NTRs were allowed to equilibriate throughout the simulation box to estimate the equilibrium one-dimensional probability distribution $P_{\mathrm{eq}(z)}$ (in contrast, the simulations in the main text were run with a non-zero steady-state flux). The effective potential (which is equivalent to the potential of mean force (3, 4)) in the pore was obtained as $U = -ln(P_{\mathrm{eq}(z)})$ (5–7).

As the FG nup density may have an effect on the effective diffusion coefficient, we measured the diffusion coefficient separately in the low density peripheral and high density central regions of the pore (demarcated in Figure S7A). For each NTR concentration, the two regions of the pore and the equilibrium number of NTRs and FG nups contained within were placed in a separate simulation box with periodic boundary conditions, so that NTRs were effectively diffusing within an infinite, rugged pipe formed by repeats of this region (Figure S7B). Despite the complex environment within the pore, we observe normal diffusion of the NTRs in the pore as illustrated in Figure S8 that shows sample MSD plots obtained separately for the central and peripheral regions within the pore (see Methods), at various concentrations. The MSDs of the NTRs were then measured, and the effect of the spatially varying effective potential within each region of the pore was removed using the Zwanzig correction (1) to the diffusion coefficient:

$$D_{\mathrm{true}} = \langle e^{U(z)} \rangle_z D_{\mathrm{app}} \langle e^{-U(z)} \rangle_z$$

where D_{true} is the true diffusion coefficient, D_{app} is the apparent diffusion coefficient obtained from the MSD measurements, and $U(z)$ is the effective potential within the region of the pore.

D. Changes in the diffusion coefficient due to crowding cannot explain the clogging-free response. Within the NPC model of this paper, due to the non-uniform shape of the pore and the differences in the cohesiveness between the peripheral and the central FG nups, the density of FG nups is non-uniform throughout the channel. This difference in FG nup density and cohesiveness along the pore results in different effective diffusion coefficients at the center and at the peripheries of the pore. Within our single-particle 1D diffusion model, the effective diffusion coefficient $D(z)$ is therefore approximated as piecewise-constant:

$$D(z) = \begin{cases} D_{\mathrm{out}}, & z < -L \\ D_{\mathrm{in}}^{\mathrm{P}}, & -L \leq z < -L^C \\ D_{\mathrm{in}}^{\mathrm{C}}, & -L^C \leq z < L^C \\ D_{\mathrm{in}}^{\mathrm{P}}, & L^C \leq z < L \\ D_{\mathrm{out}}, & L \leq z \end{cases} \quad [1]$$

where D_{out} is the diffusion coefficient outside the pore, $D_{\mathrm{in}}^{\mathrm{P}}$ is the diffusion coefficient in the peripheral regions of the pore, and $D_{\mathrm{in}}^{\mathrm{C}}$ is the diffusion coefficient in the central region of the pore. $L^C = 6.2$ nm is the boundary between the central and peripheral regions of the pore (see Supplementary Figure S7). D_{out} is given by the Stokes-Einstein equation and has no dependence on crowding. Figure 3C shows that both $D_{\mathrm{in}}^{\mathrm{P}}$ and $D_{\mathrm{in}}^{\mathrm{C}}$ are non-increasing as crowding increases.

This dependence of the diffusion coefficient on crowding could be explained by several potential effects. Increased NTR-NTR crowding creates obstruction which is expected to decrease the diffusion coefficient. Increased FG nup density increases the "stickiness" (i.e. increases the dissociation times of NTRs from the FG nups within the region), which is also expected to decrease the diffusion coefficient. Within the peripheral regions of the pore, both the NTR and FG nup density increase due to crowding, leading to a decrease in diffusion coefficient. In contrast, within the central region of the pore, crowding results in an increase in NTR density but decrease in FG nup density, so a balance between these two effects may result in a relatively constant diffusion coefficient. An alternative explanation is that the central region of the pore is crowded even at low NTR concentrations to the extent that further crowding affects the diffusion coefficient very little. Importantly, we have not observed increasing diffusion coefficients with crowding.

Furthermore, we find that the non-increasing diffusion coefficients which we measure within the pore cannot produce by themselves any of the clogging free behaviours. Equation 6 in the main text shows that decreasing $D(z)$ would lead to a decrease in flux; therefore without the changes to the effective potential, we would expect to see a saturation of the flux due to crowding. Similarly, we found that the changes in the NTR diffusion coefficient due to crowding alone do not produce increasing translocation probabilites and decreasing transport times by investigating the hypothetical case of an effective potential that did not change with crowding using Equations 3 and 4 in the main text, as shown Figure S9. We conclude that the clogging-alleviating behaviours we observe occur due to the changes of the effective potential due to crowding rather than crowding effects on the diffusion coefficients.

E. A heuristic model for the absence of the flux saturation with crowding. Assuming that the NTR distribution within the pore is almost symmetric (which is true even at nonequilibrium steady states, see Supplementary Figure S5B), and therefore approximately half of the total flux leaving the NPC exits into the nucleus. The flux can be heuristically approximated as

$$J = \frac{1}{2}\int_{z_{\mathrm{ex}}^-}^{z_{\mathrm{ex}}^+} \frac{N_{\mathrm{pore}}\widetilde{P}(z)}{\tau(z)}dz \qquad [2]$$

where $\frac{1}{\tau(z)}$ is the average rate with which NTRs starting from an initial position z escape from the NPC (in either direction). N_{pore} is the total number of NTRs within the pore, and $\widetilde{P}(z) = \frac{P(z)}{\int_{z_{\mathrm{ex}}^-}^{z_{\mathrm{ex}}^+} P(z)}$ is the 1D probability density of NTR positions within the pore, such that $N_{\mathrm{pore}}\widetilde{P}(z)$ is the expected number of NTRs within a slice dz of the pore. $\tau(z)$ is the average residence time, given as the mean first passage time to escape through either pore opening (8–10):

$$\tau(z) = \int_{z}^{z_{\mathrm{ex}}^+} \left[\frac{e^{U(z')}}{D(z)}\int_0^{z'} e^{-U(z'')}dz''\right]dz' \qquad [3]$$

The results of this model are shown in the main text in Figures 2C and 4A ("τ approx" lines).

F. An NPC model containing only low cohesion FG nups cannot produce an anti-clogging regime. The case of an NPC filled with only low cohesion FG nups is somewhat more complicated than the NPC filled with only high cohesion FG nups. As shown in Figure S10A we observe two distinct regimes of the dependence of the translocation dynamics on crowding at low and high NTR concentrations. At low NTR concentrations both translocation probabilities and transport times increase with NTR concentration. The qualitative explanation for this effect is that due to the low cohesion of the FG nups the density of FG nups inside the pore is low in the absence of NTRs. As the number of NTRs inside the pore increases, their interaction with FG nups initially draws more nups into the pore, deepening the effective potential in the pore and leading to the increase in both translocation probabilities and transport. At high concentrations, the FG nups are already collapsed into the pore and the effect of competition between NTRs begins to dominate, making the effective potentials shallower as crowding increases. This leads to a decreasing translocation probability with crowding, and transport times that initially drop and then gradually increase, likely due to jamming (10). Notably, we do not observe an anti-clogging regime with increasing translocation probability and simultaneously decreasing transport times neither at the high nor at the low concentration regimes.

G. Interchangeability of "slow" and "fast" NTRs within FG nup assemblies. In Section 2E we observed a biphasic decay of NTRs within the pore which was consistent with previous observations of "fast" and "slow" NTR populations (11–14).

We wanted to further understand whether the "fast" and "slow" groups were dynamically distinct populations predisposed to escaping at different rates, or if the composition of these groups was random.

To this end, we first identified the NTRs which were among the first 20 to leave the pore as the "fast" group, and the NTRs which had been among the last 20 to leave the pore as the "slow" group (out of the initial 150 NTRs in the pore). We then ran short simulations to sample 100 random realizations of the early stages of our emptying pore, using the same initial conditions and changing only the seed of the random number generator, and recorded the identities of the first five NTRs to escape each time.

We found that NTRs identified as members of the group of 20 "fast" NTRs and the group of 20 "slow" NTRs in the initial simulation were equally likely to be among the first five to leave in the alternative realizations of the simulation. This is quantified in Figure S11 which shows that the proportion of the alternate realizations where n NTRs from the "fast" or "slow" groups were among the first 5 to escape agrees with the binomial distribution $\mathcal{B}(n, p)$ where p is the probability of randomly selecting an NTR from the "fast" or "slow" groups by picking any NTR initially within the pore. Therefore NTRs from the originally identified "fast" group are not more likely to escape the pore first compared to NTRs which were not from this group. This therefore indicates that the "fast" and "slow" groups cannot be identified *a priori*, but are formed dynamically as the pore empties.

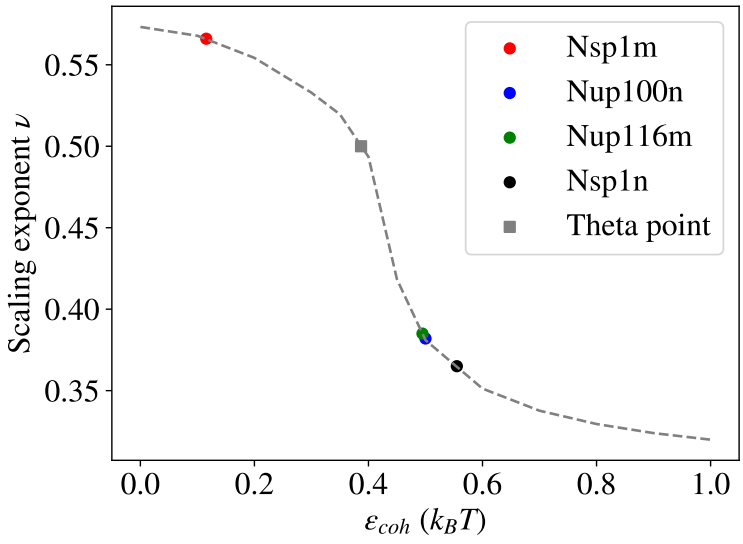

Fig. S1. FG nup cohesion calibration: The scaling parameter ν determines the average linear dimension of the polymer through $R \propto N^{\nu}$, quantified here as the radius of gyration. Here we show the experimentally determined scaling exponents of select FG nups (15, 16) and the corresponding ϵ_{coh} values in our simulation setup. The cohesiveness of the peripheral FG nups in our NPC model was $\epsilon_{\text{coh}} = 0.3\ k_BT$, and $\epsilon_{\text{coh}} = 0.5\ k_BT$ for the central FG nups. These values were chosen to lie on opposite sides of the coil-globule transition ("theta point"), reflecting the two types of conformations found in FG nups (15).

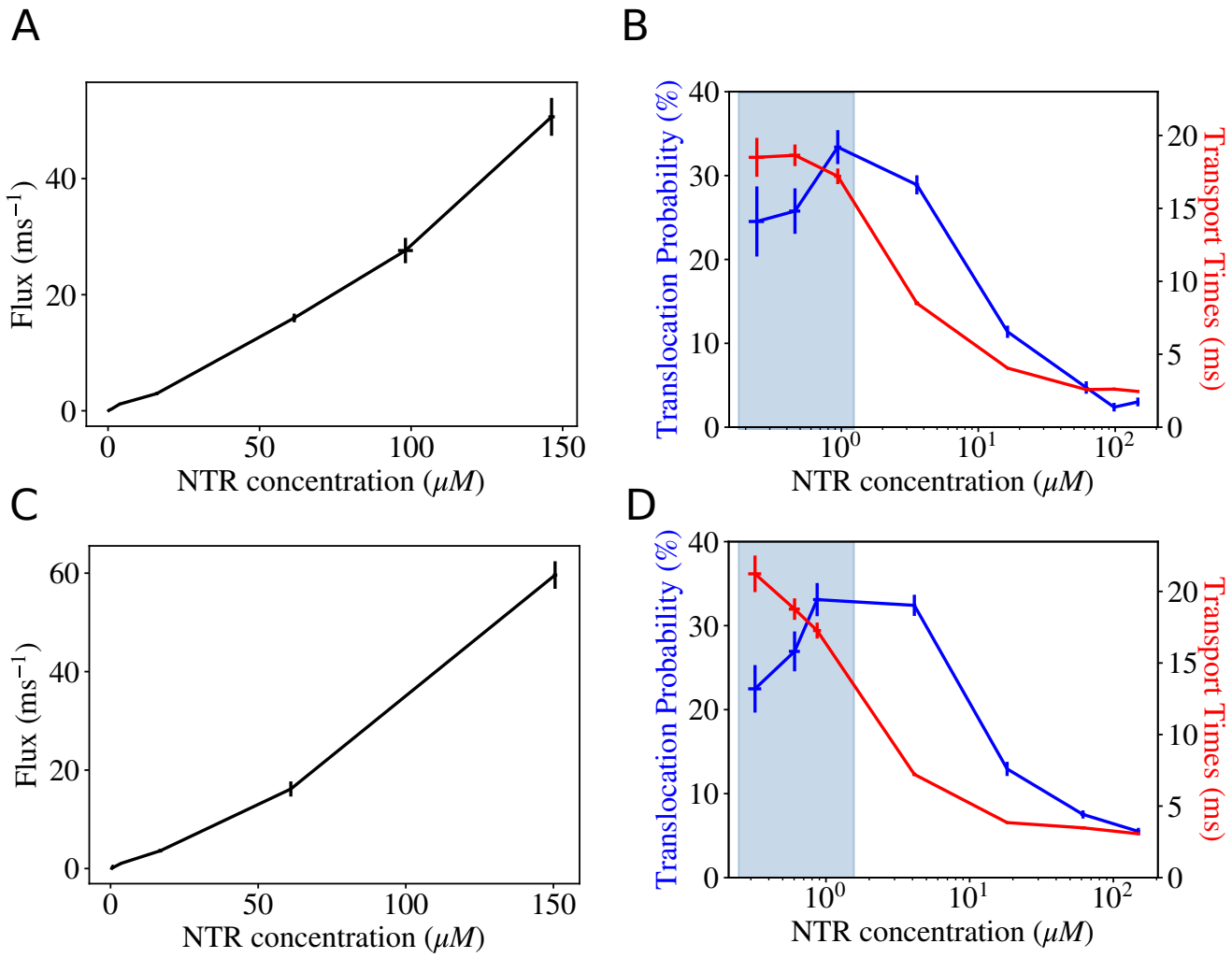

Fig. S2. The absence of flux saturation and the anti-clogging regime persist in alternative versions of the model. (A) and (B) The flux, translocation probabilities, and transport times in the case with weakly attractive interaction between NTRs. (C) and (D) The flux, translocation probabilities, and transport times in the case where only 75% of NTRs reaching the boundary of the simulation box on the nuclear side is absorbed. Blue shading highlights the anti-clogging regimes.

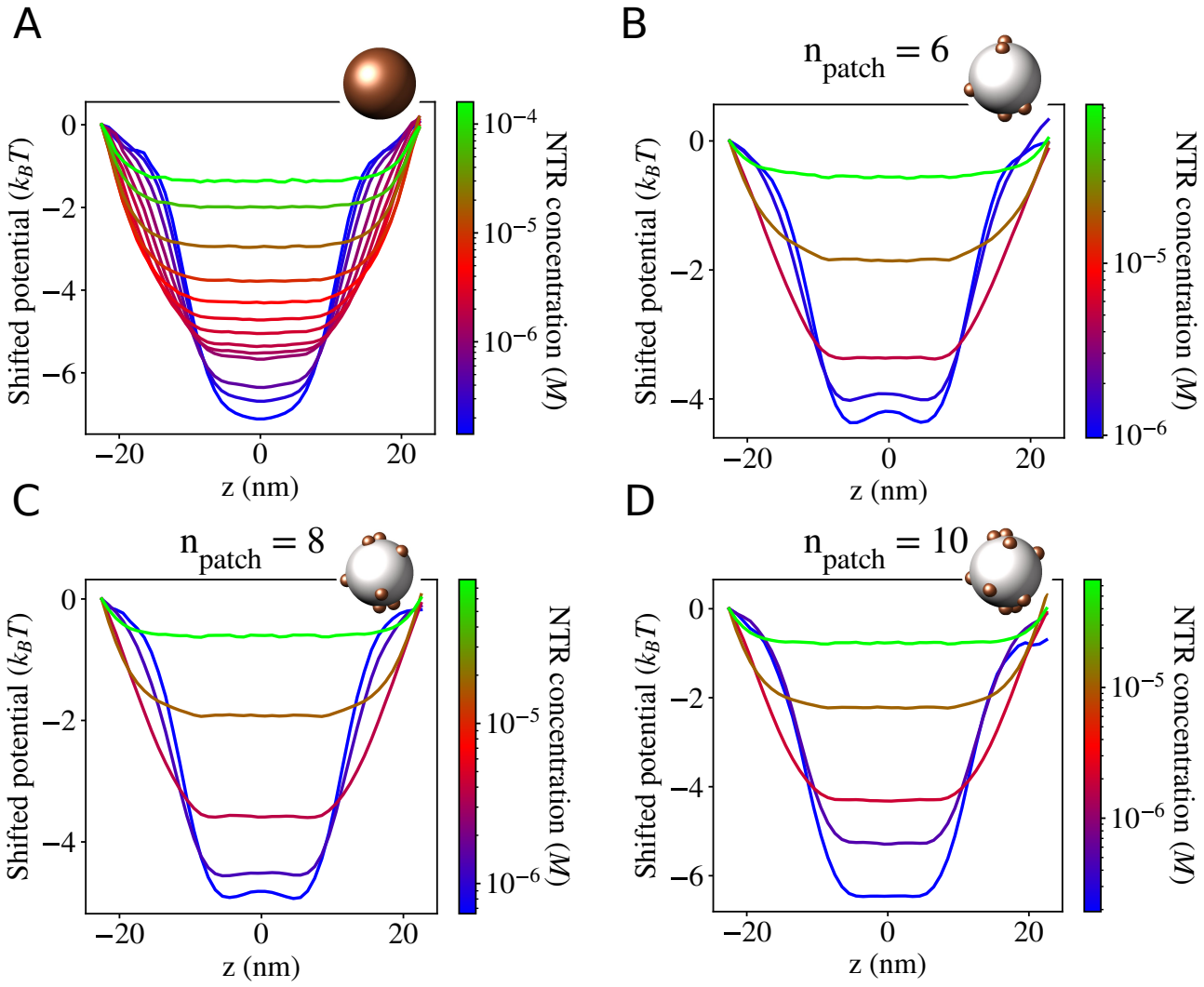

Fig. S3. Discrete binding sites on NTRs do not result in rougher potentials inside the pore. All panels zoom in to show the effective potential within the pore (between z_{ex}^- and z_{ex}^+), and are shifted to align at 0 at z_{ex}^- for ease of visual comparison. (A) Shifted potentials corresponding to the uniform NTR model used in the main text. (B) Shifted potentials with an NTR with $n = 6$ binding patches, each with an attractive interaction with FG nups of $\epsilon_{attr} = 2.4\ k_BT$. (C) Shifted potentials with an NTR with $n = 8$ binding patches, each with an attractive interaction with FG nups of $\epsilon_{attr} = 2.0\ k_BT$. (D) Shifted potentials with an NTR with $n = 10$ binding patches, each with an attractive interaction with FG nups of $\epsilon_{attr} = 1.8\ k_BT$. The shifted potentials in panels B-D show similar behavior to panel A in the presence of crowding, with the potential decreasing in depth with increased crowding.

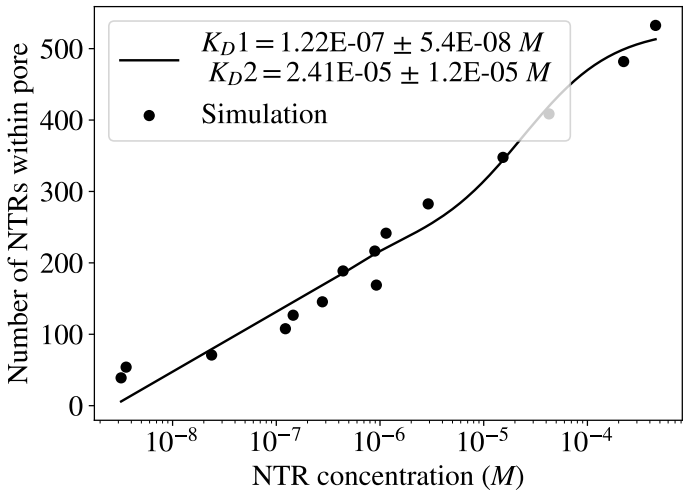

Fig. S4. Our NPC model displays strong thermodynamic selectivity for NTRs. The accumulation of NTRs in our NPC model is fit by a 2-component Langmuir model producing $K_{D_1} = 1.2 \times 10^{-7}\ M$ and $K_{D_2} = 2.4 \times 10^{-5}\ M$. These values agree well with experimentally measured values (17). However, the bulk flux through our NPC model does not saturate even at concentrations well above both of these K_D values.

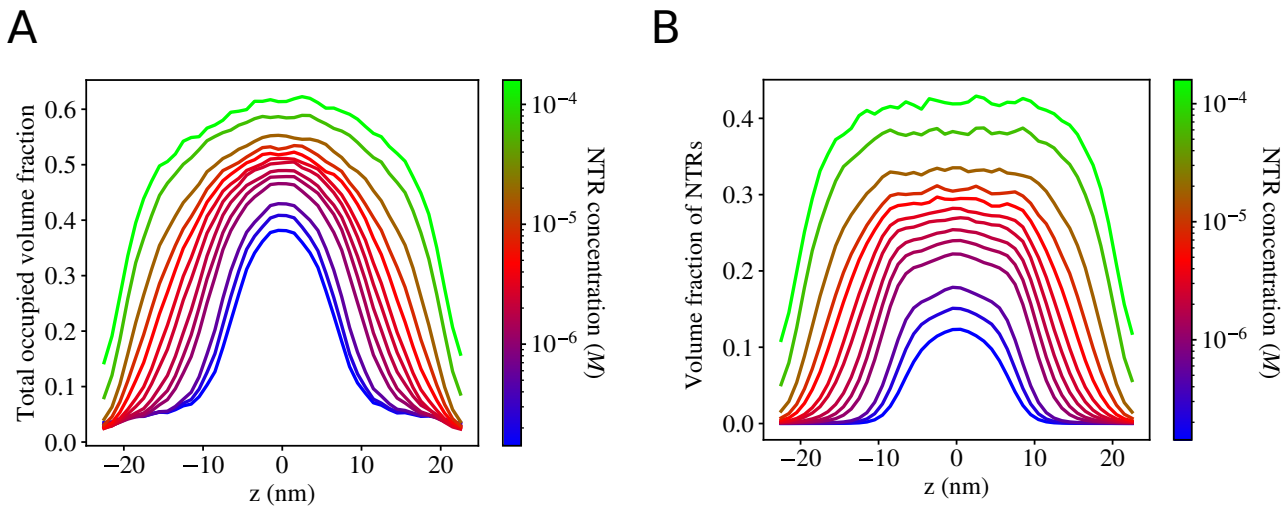

Fig. S5. Volume fractions of NTRs and FG nups within the pore. (A) The total volume fraction occupied by FG nups and NTRs within our simulation reaches more than 0.6 in parts of the pore, which is close to the close random packing densities of 0.62-0.64. Despite such a crowded interior, we observe no saturation of the flux through the NPC or increase in the transport times. (B) The distribution of NTRs within the pore at steady-state is almost symmetric for NTR concentrations, allowing us to make simplifying assumptions in the derivation of Equation 2.

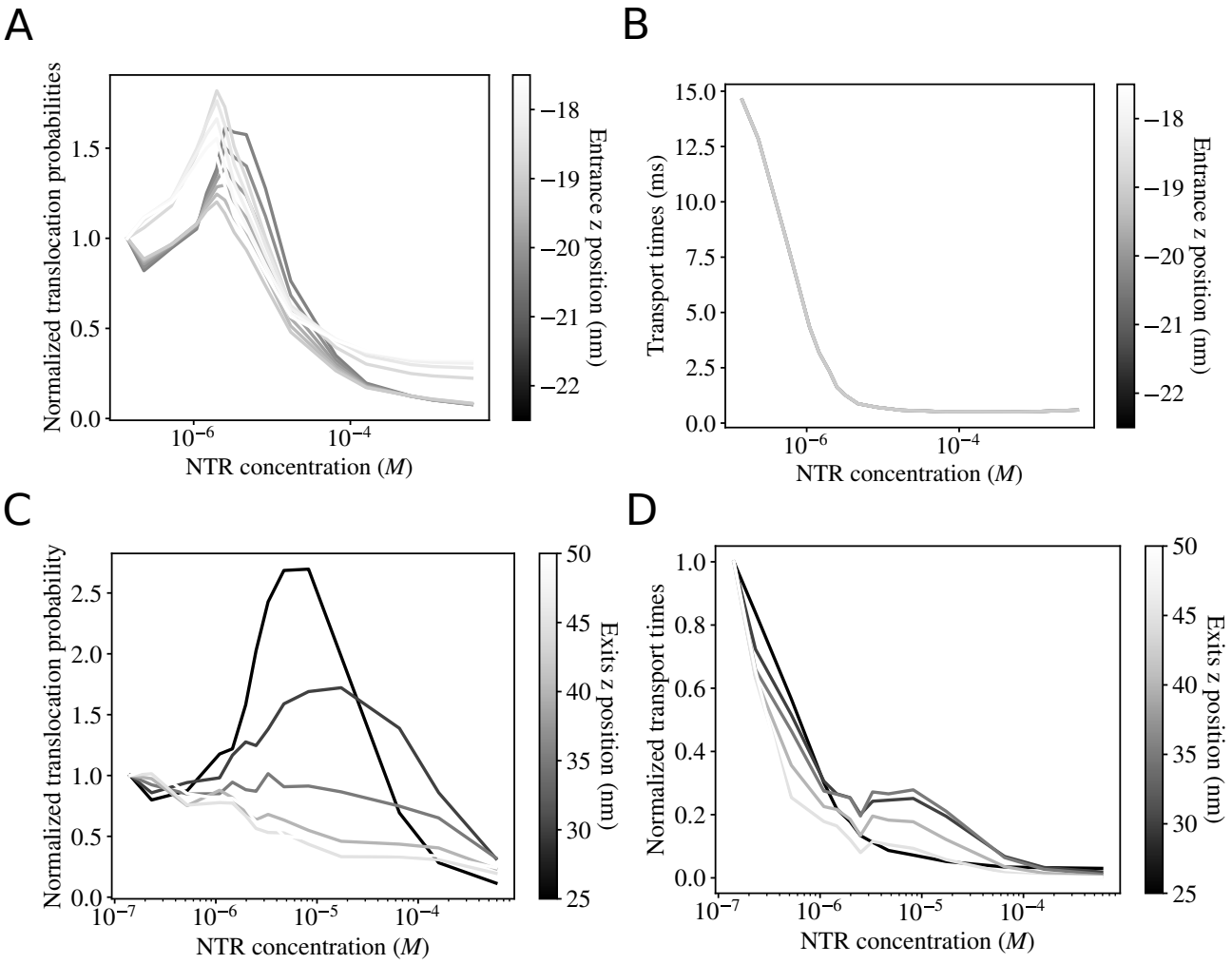

Fig. S6. Testing the alternative definitions of the start and the finish of a translocation attempt. The nuclear envelope extends between $z = \pm 20$ nm. (A) Translocation probabilities for different entrance positions, with values normalized by the translocation probability at the lowest NTR concentration. (B) Differences in the transport times using different choices of the entrance positions are negligible. (C) Translocation probabilities for different choices exit positions, with values normalized by the translocation probability at the lowest NTR concentration. The choice of exit positions is always symmetric such that $-z_{\text{ex}}^{-} = z_{\text{ex}}^{+}$. In all simulations an NTR was consideded to have entered the NPC when its center reached one diameter to the right of the cytoplasmic exit location. (D) Transport times for different choices of the exit positions, normalized by the times at the lowest NTR concentration.

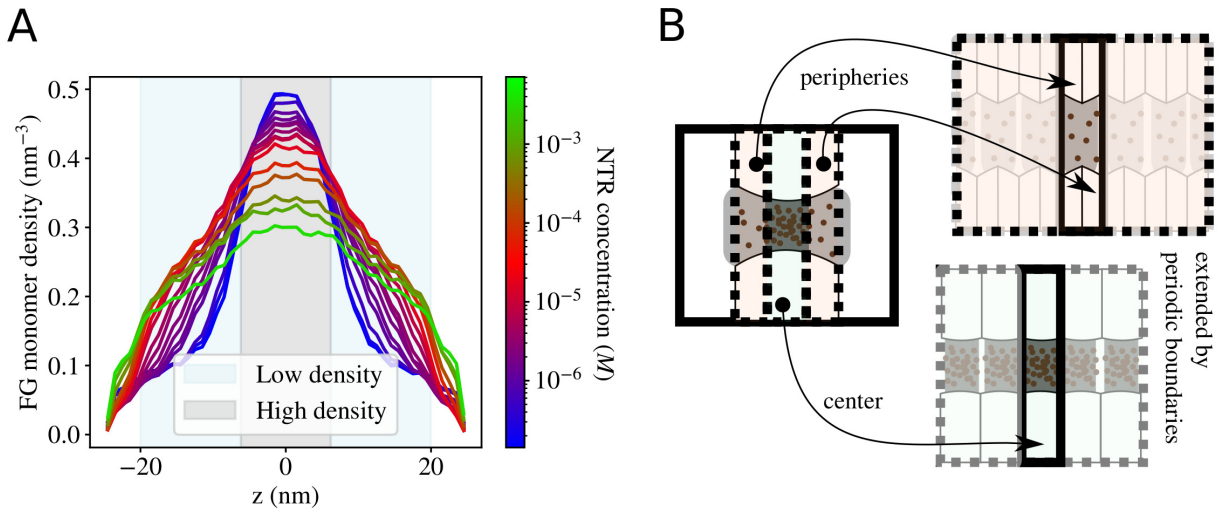

Fig. S7. The setup for measuring the effective diffusion coefficients from simulations. (A) To account for the differences in FG nup densities at different regions within the pore, the diffusion coefficients were measured separately for the central (grey) and peripheral (blue) regions of the pore. (B) For each NTR concentration, the central and peripheral regions of the pore (and the NTRs contained within) were each placed in a separate simulation box with periodic boundary conditions, and the MSDs of the NTRs were measured within these infinite, irregular channels.

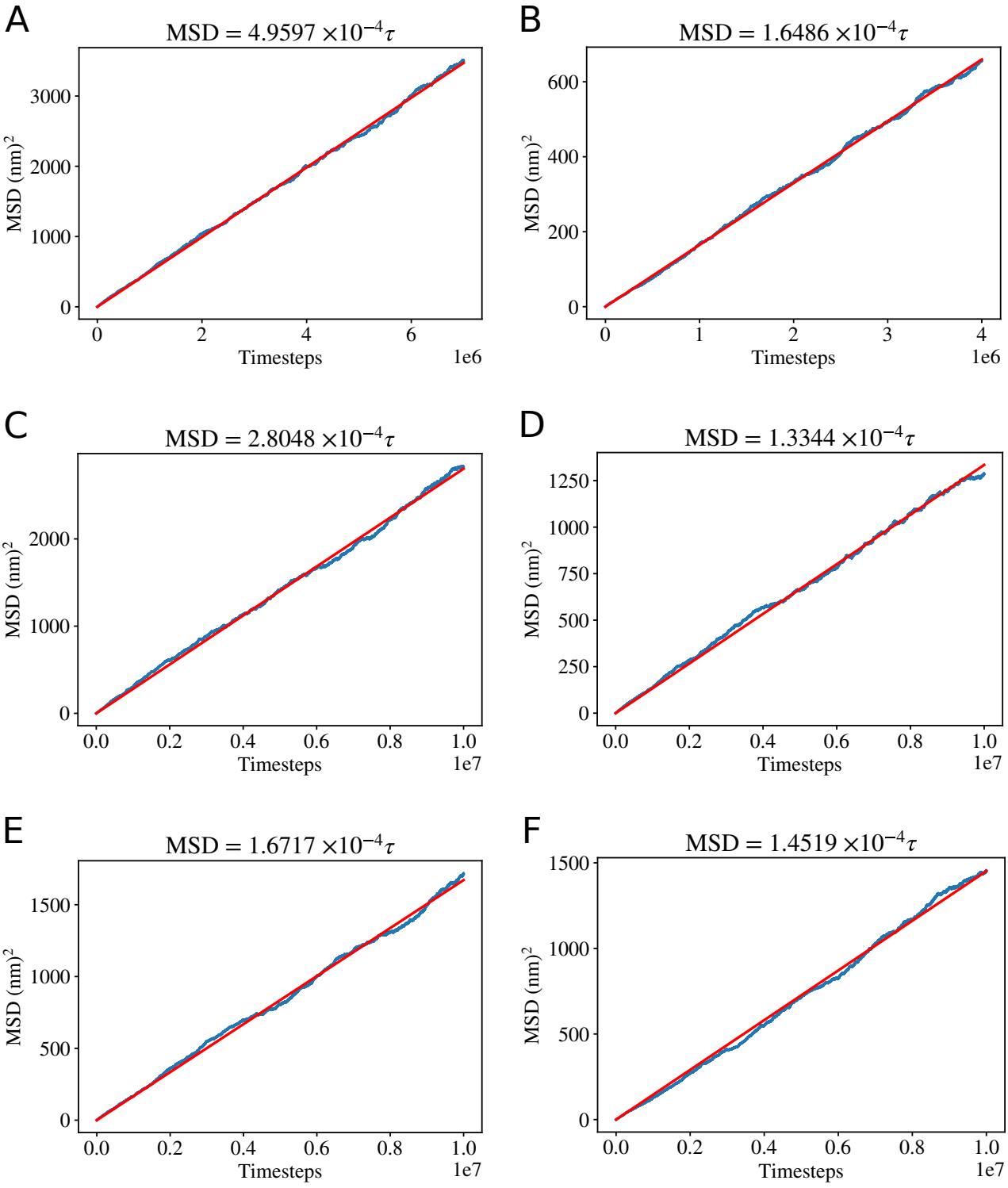

Fig. S8. Sample MSD measurements within the central and peripheral regions of the pore at different NTR concentrations. (A) MSD measured in central region of the pore, NTR concentration $= 1.42 \times 10^{-7} M$. (B) MSD measured in peripheral region of the pore, NTR concentration $= 1.42 \times 10^{-7} M$. (C) MSD measured in central region of the pore, NTR concentration $= 2.49 \times 10^{-6} M$. (D) MSD measured in peripheral region of the pore, NTR concentration $= 2.49 \times 10^{-6} M$. (E) MSD measured in central region of the pore, NTR concentration $= 1.60 \times 10^{-4} M$. (F) MSD measured in peripheral region of the pore, NTR concentration $= 1.60 \times 10^{-4} M$.

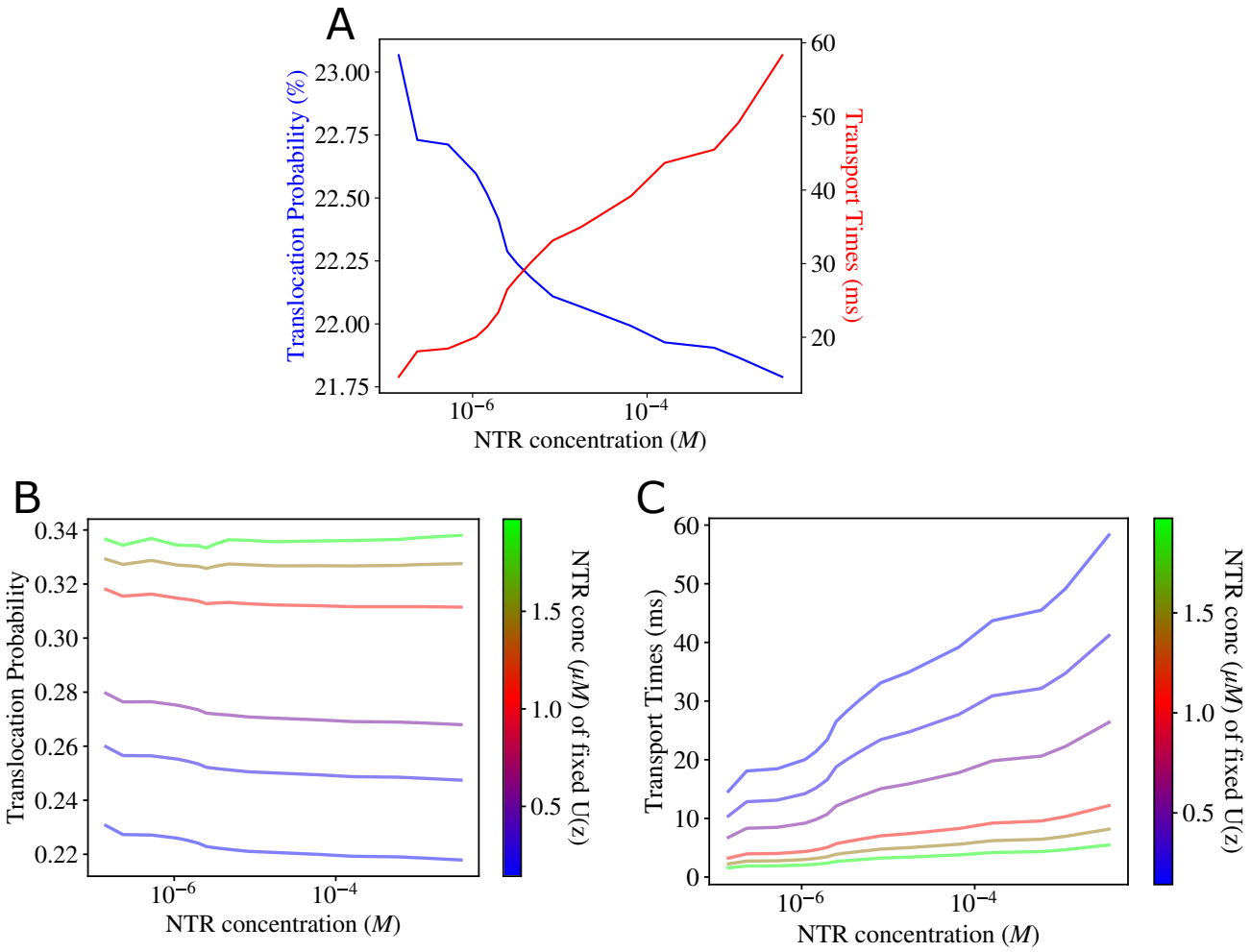

Fig. S9. Measured changes in the effective diffusion coefficient cannot produce increasing translocation probabilities or decreasing transport times in the absence of changes in the effective potential. (A) The translocation probabilities and transport times predicted by the Fokker Planck model (Equations 3 and 4 from the main text) where only $D(z, \text{conc})$ has a dependence on NTR concentration (as measured in simulations); the effective potential $U(z, \text{conc})$ is replaced with $U(z, \text{conc} = 0.1\mu M)$ to remove the concentration dependence of the effective potential. In the absence of crowding induced changes in the effective potential, the changes in the diffusion coefficient do not produce the anti-clogging regime or decreasing translocation times. (B) and (C) For completeness, we repeat the procedure in (A), but replacing $U(z, \text{conc})$ with $U(z, \text{conc} = c_i)$ with c_i in the concentration range of the anti-clogging regime of the full simulations in the main text. The dependence of the diffusion coefficient on crowding is not sufficient to produce translocation probabilities that increase, and transport times that decrease with crowding.

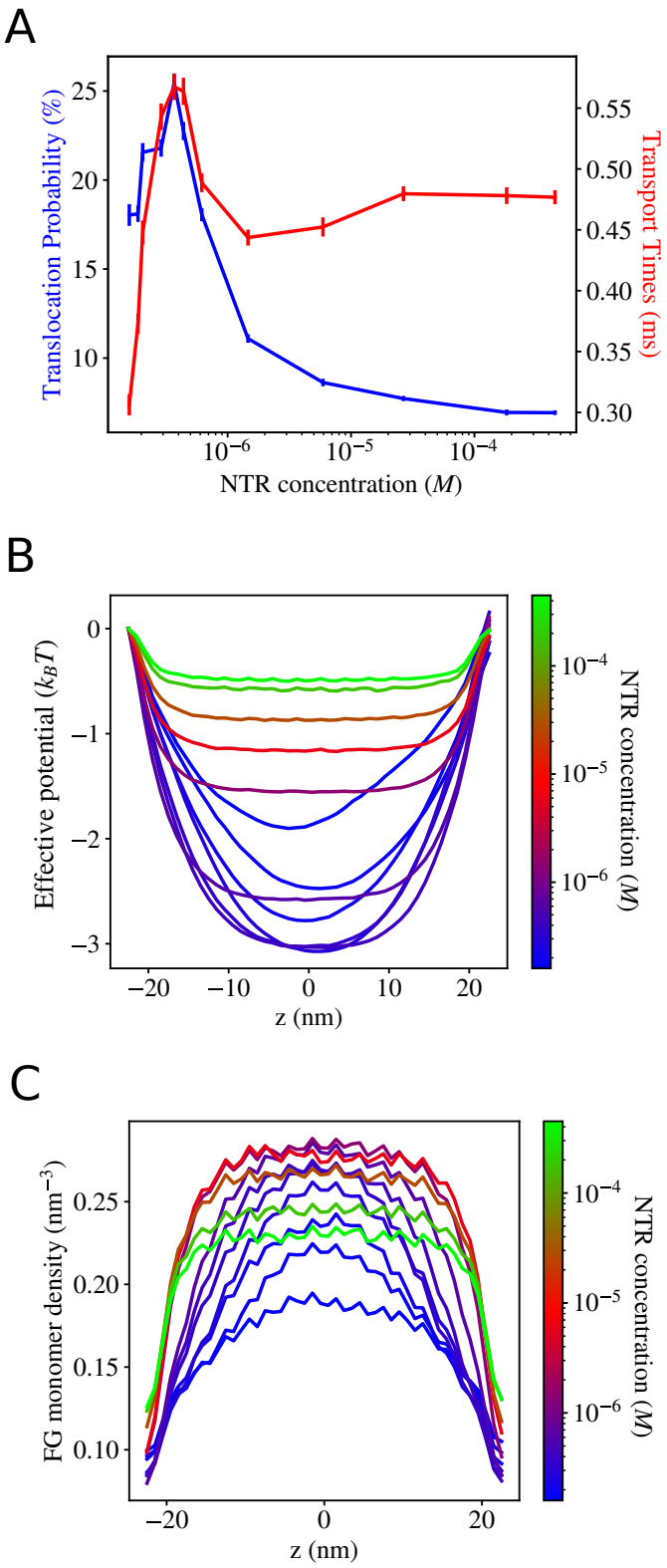

Fig. S10. Simulation results for an NPC filled with only low cohesion FG nups. (A) Translocation probabilities and transport times. (B) The effective potentials within the pore, relative to the potential at the cytoplasmic exit. As the NTR concentration increases, the effective potential deepens (blue to light purple), then becomes shallower (light purple to green). (C) As the NTR concentration increases, the density of the FG nups within the pore first increases (blue to purple), then decreases (purple to green) as they are squeezed out of the pore.

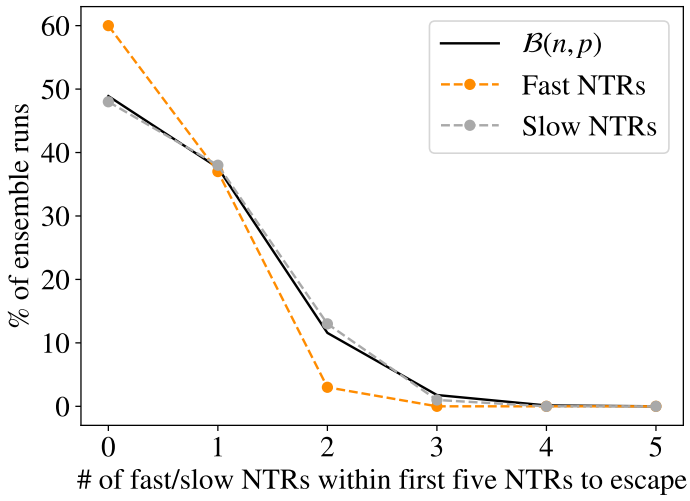

Fig. S11. Repeated sampling of the first five NTRs to leave the NPC yields similar distributions for NTRs from the original "fast" and "slow" groups identified in our initial, full-length simulation, see text. The proportion of the 100 ensemble runs where n "fast" or "slow" NTRs were observed among the first five to escape is well approximated by the binomial distribution resulting from the hypothesis that all NTRs initially within the pore are equally likely to escape.

References

1. R Zwanzig, Diffusion in a rough potential. *Proc. Natl. Acad. Sci.* **85**, 2029–2030 (1988).
2. W Yang, SM Musser, Nuclear import time and transport efficiency depend on importin β concentration. *The J. cell biology* **174**, 951–961 (2006).
3. D Winogradoff, HY Chou, C Maffeo, A Aksimentiev, Percolation transition prescribes protein size-specific barrier to passive transport through the nuclear pore complex. *Nat. communications* **13**, 1–16 (2022).
4. C Gu, RD Coalson, D Jasnow, A Zilman, Free energy of nanoparticle binding to multivalent polymeric substrates. *The J. Phys. Chem. B* **121**, 6425–6435 (2017).
5. R Zwanzig, Diffusion past an entropy barrier. *The J. Phys. Chem.* **96**, 3926–3930 (1992).
6. P Kalinay, J Percus, Projection of two-dimensional diffusion in a narrow channel onto the longitudinal dimension. *The J. chemical physics* **122**, 204701 (2005).
7. A Berezhkovskii, M Pustovoit, S Bezrukov, Diffusion in a tube of varying cross section: Numerical study of reduction to effective one-dimensional description. *The J. chemical physics* **126**, 134706 (2007).
8. AW Lau, TC Lubensky, State-dependent diffusion: Thermodynamic consistency and its path integral formulation. *Phys. Rev. E* **76**, 011123 (2007).
9. CW Gardiner, , et al., *Handbook of stochastic methods.* (springer Berlin) Vol. 3, (1985).
10. A Zilman, J Pearson, G Bel, Effects of jamming on nonequilibrium transport times in nanochannels. *Phys. review letters* **103**, 128103 (2009).
11. RY Lim, B Huang, LE Kapinos, How to operate a nuclear pore complex by kap-centric control. *Nucleus* **6**, 366–372 (2015).
12. T Jovanovic-Talisman, et al., Artificial nanopores that mimic the transport selectivity of the nuclear pore complex. *Nature* **457**, 1023–1027 (2009).
13. LE Kapinos, RL Schoch, RS Wagner, KD Schleicher, RY Lim, Karyopherin-centric control of nuclear pores based on molecular occupancy and kinetic analysis of multivalent binding with fg nucleoporins. *Biophys. journal* **106**, 1751–1762 (2014).
14. A Fragasso, et al., Transport receptor occupancy in nuclear pore complex mimics. *Nano Res.* pp. 1–15 (2022).
15. J Yamada, et al., A bimodal distribution of two distinct categories of intrinsically disordered structures with separate functions in fg nucleoporins. *Mol. & Cell. Proteomics* **9**, 2205–2224 (2010).
16. A Vovk, et al., Simple biophysics underpins collective conformations of the intrinsically disordered proteins of the nuclear pore complex. *Elife* **5**, e10785 (2016).
17. J Kalita, et al., Karyopherin enrichment and compensation fortifies the nuclear pore complex against nucleocytoplasmic leakage. *J. Cell Biol.* **221**, e202108107 (2022).